Optimization of heterogeneous photoelectrocatalysis on nanotubular TiO_2 electrodes: Reactor configuration and kinetic modelling

Andrea Turolla [a], Massimiliano Bestetti [b,c], Manuela Antonelli [a,*]

[a] *Politecnico di Milano, Department of Civil and Environmental Engineering - Environmental Section, Piazza Leonardo da Vinci 32, 20133 Milano, Italy* [b] *Politecnico di Milano, Department of Chemistry, Materials and Chemical Engineering "G. Natta", Via Mancinelli 7, 20131 Milano, Italy*
[c] *Institute of Physics and Technology, Tomsk Polytechnic University, Lenin Avenue 2a, Tomsk 634050, Russia*

Photoelectrocatalytic degradation of target molecules on nanotubular titanium dioxide (TiO_2) immobi-lized on meshed conductive substrate was assessed by measuring the photoelectrochemical response (i.e., generated photocurrent) as indicator of TiO_2 performance. Furthermore, a simple and reliable methodology for degradation modelling and laboratory reactor optimization has been proposed and validated. Nanotubular TiO_2 was grown by anodic oxidation of Ti wire meshes and characterized by ESEM and XRD. Immobilized TiO_2 on Ti wire mesh was used as photo-anode under UV irradiation (254 nm) and subjected to electrical polarization. The photocurrent was monitored in a three-electrode cell, by varying polarization voltage, TiO_2 electrode relative positioning to the UV source (distance), and concentration of a model azo dye compound (Reactive Red 243, RR243). Photoelectrochemical response was modelled as a function of operating parameters and guidelines for photoreactor configuration were identified. Optimized batch photoreactor configuration (1.8 L) was used for degrading a 25 mg L^{-1} RR243 aqueous solution, achieving 90% decolorization in 45 min and 60% mineralization in 100 min. Decolorization kinetics were effectively described by means of a modified Langmuir-Hinshelwood model based on experimentally measured photocurrents, accounting for the dynamic behaviour of the process due to the change in solution transmittance over time determined by the degradation of target compounds.

Keywords:
Advanced oxidation processes Photoelectrocatalysis
TiO_2nanotube array electrodes Langmuir-Hinshelwood kinetic model

1. Introduction

Titanium dioxide (TiO_2) photoelectrocatalysis is one of the most innovative processes for water and wastewater treatment, since semiconducting properties of TiO_2 make it an excellent material for advanced oxidation (Fujishima et al., 2008; Garcia-Segura and Brillas, 2017; Pichat, 2013). Some relevant challenges in the development of affordable technological solutions are related to the improvement of process yields and to TiO_2 immobilization, having the objective of making the process competitive with other industrially established technologies, such as ozonation or

* Corresponding author.
E-mail address: manuela.antonelli@polimi.it (M. Antonelli).

Published Journal Article available at: https://doi.org/10.1016/j.ces.2018.02.041

advanced oxidation based on the photolysis of hydrogen peroxide by means of UV radiation (Choi et al., 2010; Chong et al., 2010).

Heterogeneous photoelectrocatalysis on immobilized nanotubular TiO_2 electrodes is a valuable alternative that significantly reduces some of the main process drawbacks based on dispersed TiO_2 nanopowders. In fact, TiO_2 is grown directly on Ti by anodic oxidation in form of self-ordered nanotube arrays with relatively high specific surface area (about 30 $m^2 g^{-1}$) (Roy et al., 2011) and it may be biased due to good backside electrical contact provided by the metallic substrate (Mor et al., 2006; Zhang et al., 2012). Therefore, a separation stage by filtration of TiO_2 photocatalyst after treatment is not required, being one of the most relevant issues for process engineering in case of photocatalysis on TiO_2 suspensions in slurry phase (De Lasa et al., 2005). Furthermore, TiO_2 anodic polarization allows to scavenge the electrons promoted in the conduction band through the electrical circuit and, thus, to reduce the electron-hole pairs recombination, for which a significant part of the separated charges on TiO_2 surface is usually lost (Egerton and Christensen, 2004). This results in a strong positive effect on process yield, as already demonstrated by several studies (Macak et al., 2007; Zlamal et al., 2007).

In recent years, nanotubular TiO_2 electrodes are being widely studied for a number of applications, among which sustainable energy production, as hydrogen generation from water splitting and new generation photovoltaic solar panels (Meng et al., 2011; Zhu et al., 2007). With respect to investigations related to the energy sector, the research for water and wastewater treatment was limited and relatively few studies have been conducted on nan-otubular TiO_2 photoelectrocatalysis for the removal of organic com-pounds so far, as 4-chlorophenol (Wang et al., 2009), aromatic amines (Cardoso et al., 2010), bisphenol A (Brugnera et al., 2010), methyl orange (José Martín de Vidales et al., 2016), methylene blue (Cheng et al., 2013), metoprolol (Ye et al., 2018), pentachlorophenol (Quan et al., 2007), salicylic acid (Zhang et al., 2014). Two common features of the just-mentioned papers, also valid for other forms of immobilized TiO_2, are the proof-of-concept scale and the strong interest in nanomaterial synthesis, while the influence of operating parameters on process performance and strategies for photoreactor configuration have been poorly investigated, although they are strongly required in the view of process optimization and scale-up.

In fact, though a number of configurations for the application of immobilized TiO_2 have been proposed in the past (De Lasa et al., 2005; Leblebici et al., 2015; Litter, 2009; Pichat, 2013), a systematic methodology for the design of optimized scaled-up photoreactors is still lacking. In particular, advances are hindered by process complexity, whose mechanistic modelling asks for the description of many interacting chemical-physical phenomena, including fluid dynamics, mass transport, radiation transfer and chemical reactions. While most of related literature relies on simplified approaches using the coefficients of pseudo-kinetic models referred to the degradation of target pollutants as unique indica-tors, several attempts were carried out for the mechanistic mod-elling of photocatalysis on immobilized TiO_2, *inter alia* Duran et al. (2011) and Vezzoli et al. (2011). However, both being both approaches characterized by relevant drawbacks. As for pseudo-kinetic models, it is usually difficult to get generalizable outcomes to be applied to reactor configuration; on the other hand, mecha-nistic modelling is often an intricate task, needing for powerful numerical tools for managing the multi-physical framework.

A viable alternative consists in the identification of proxy variables describing the overall photoreactor behaviour, that act as indicators of photocatalytic fundamental processes (e.g., the extent of immobilized TiO_2 photoactivation or the generation of reactive species) and that can be determined by easy and reliable experimental measures. In this regard, photoelectrocatalysis presents an important plus with respect to photocatalysis, since TiO_2 photoactivation can be evaluated by measuring the generated photocurrent, which is a direct consequence of charge separation at photocatalyst surface (Jennings et al., 2008; Varghese and Grimes, 2008). This method, commonly used in other TiO_2-based applications as photo-assisted water electrolysis cells and dye-sensitized solar cells, can be effectively adopted also for evaluating TiO_2 photoactivation in reactors for water and wastewater treatment, as demonstrated at laboratory scale (Pablos et al., 2013). Assuming that a better TiO_2 photoactivation corresponds to a higher rate of reactive species generation, and hence to higher overall degradation yield, it is possible to determine the influence of operating parameters and to optimize the process by maximizing TiO_2 photoactivation in terms of photocurrent. In conclusion, photocurrent could be assumed as a measurable proxy variable for TiO_2 photoactivation which a simple and reproducible methodology for process optimization and reactor configuration could be based on.

In the present research work the influence of reactor configuration and various operating parameters on the performance of photoelectrocatalysis on nanotubular TiO_2 immobilized on meshed conductive substrate has been evaluated, using photoelectrochemical response (i.e., generated photocurrent) as an indicator of TiO_2 photoactivation. In particular, the effect of polarization voltage, TiO_2 electrode relative positioning to the UV source (distance) and concentration of a model azo dye compound (Reactive Red 243) was assessed in a three-electrode cell, in which nanotubular TiO_2, grown by anodic oxidation of wire Ti meshes, was used as photoanode under UV irradiation and subjected to electrical polarization. The ultimate objective of the research work was to model photoelectrochemical response as a function of operating parameters and to identify guidelines for photoreactor configuration in order to develop an optimized photoreactor configuration at the laboratory scale. The photocurrent values were used for modelling the decolorization kinetics in the view of effectively describing the dynamic behaviour of the process due to changes in the operating conditions over time.

2. Material and methods

2.1. Preparation and structural characterization of nanotubular TiO_2

A commercially pure titanium (Ti grade 1) expanded metal was used as substrate. Nanostructured TiO_2 was grown by anodic oxidation of titanium in fluoride containing solutions (1 M H_2SO_4, 0.075 M HF), by using the procedure described in Turolla et al. (2012). Anodic oxidation process lasted 24 h, during which the voltage was kept constant at 20 V, the temperature at 10 °C and the electrolyte solution was stirred by nitrogen bubbling. After anodic oxidations, an annealing phase in air at 400 °C lasting 180 min was carried out, to crystallize the amorphous TiO_2 in ana-tase form. All reagents required for the preparation of nanotubular TiO_2 were purchased from Sigma Aldrich.

Two types of TiO_2/Ti samples were anodized: square (5 × 5 cm - photoelectrochemical tests) and cylindrical (H = 40 cm, Ø = 4.5 cm - degradation tests). A graphite sheet (10 × 5 cm) was used as cathode for the anodic oxidation of square samples, while in the other case a graphite bar (Ø = 1.5 cm) coaxial to cylindrical samples was used.

Nanotubular TiO_2 morphology and its crystalline structure were characterized respectively by Environmental Scanning Electron Microscope (ESEM, Zeiss EVO 50 EP) and X-ray Diffractometer (XRD, Philips PW-1830), before and after the annealing treatment.

2.2. Dye solutions

A textile organic azo dye, Reactive Red 243 (RR243), purity 95%, was purchased from Clariant and selected as model compound for

organic pollutants, being its molecular structure shown in Fig. 1, as provided by the manufacturer. RR243 solutions were prepared by dosing various amounts of powder in deionized water. RR243 has three characteristic absorbing wavelengths at 287, 515 and 545 nm: calibration lines at these wavelengths were obtained by using standard solutions at various dye concentrations (limit of detection 0.25 mg L^{-1}). Both for photoelectrochemical and degradation tests, the initial concentration of RR243 solutions ranged between 5 and 25 mg L^{-1} and potassium chloride (KCl, Sigma Aldrich) was added at 313 mg L^{-1} to adjust initial conductivity at 635 ± 15 μS cm^{-1}, typical of drinking waters in Milan area. No significant modifica-tions in solution conductivity were determined by RR243 addition.

2.3. Photoelectrochemical tests on nanotubular TiO_2

Chrono-amperometric measurements in presence and absence of irradiation were performed in a three-electrode cell (Fig. 2a). The TiO_2/Ti square photo-anodes were inserted in a polypropylene cell (6 L volume). Titanium activated expanded metal (13 × 7 cm) and Ag/AgCl electrode were respectively used as counter and reference electrodes. A low-pressure Hg vapour UV lamp (15 W, Helios Italquartz) was used as radiation source and placed in a quartz sleeve vertically positioned in the cell (Ø = 3.4 cm). UV lamp emission spectrum was quasi-monochromatic, whose distribution is a normal curve with mean of 254 nm and standard deviation of 10 nm.

Two types of tests were performed to evaluate the photocurrent: (A) potentiostatic, by means of a potentiostat AMEL 549 and two multimeters TTi 1604, respectively used as galvanometer and potentiometer; (B) potentiodynamic, using a potentiostat/galvanostat EG&G 273/A (Princeton Applied Research). Current was measured with a time step of 1 s, while current density was then calculated as the current divided by the apparent surface area of TiO_2 electrodes, estimated as detailed below.

Potentiostatic tests lasted 360 s: the first 60 s were carried out in dark condition and the remaining time under irradiation. Photocurrent density was calculated as the difference between the mean values of current density measured in the last 60 s of light condition and the first 60 s of dark condition. Potentiostatic tests were carried out varying the following operating conditions:

(1) polarization voltage: 0, 0.5 and 1.5 V vs. Ag/AgCl,
(2) TiO_2/Ti sample - UV lamp distance: measures were performed at 1, 2, 3, 4, 5, 7 and 9 cm far from the UV lamp and the sample, being the sample positioned frontally, as shown in Fig. 2a,
(3) RR243 concentration: 0, 5, 10, 15, 20 and 25 mg L^{-1}.

In total, 126 combinations of the operating parameters were tested.

Potentiodynamic tests lasted 45 min and were repeated twice, in light and dark. Tests were carried out by linearly increasing (0.916 mV s^{-1}) the polarization voltage from 0 to 2.5 V vs. Ag/AgCl electrode. TiO_2/Ti sample was positioned at 1 cm from the UV lamp and frontally oriented. RR243 solution concentration was fixed at 25 mg L^{-1}. Tests were repeated in the same conditions using a platinum wire as the anode instead of the TiO_2/Ti sample, representative of the standard reduction potential for the development of hydrogen in the cell. In total, 3 tests were performed.

In photoelectrochemical tests solution absorbance (254, 287, 515 and 545 nm), conductivity and pH were monitored before and after each trial. The absence of significant RR243 degradation was verified in any operating condition, indicating the stability of the solution optical properties.

2.4. Photoelectrocatalytic degradation tests

As for photoelectrocatalytic degradation tests, a cylindrical TiO_2/Ti surface was used and disposed coaxially with respect to the UV lamp, the same used in photoelectrochemical tests, and both were centrally immersed in a 1.8 L Pyrex glass reactor (H = 55 cm, Ø = 8 cm) (Fig. 2b). Cylindrical TiO_2/Ti surface was biased at 1.5 V vs. Ag/AgCl with an AMEL 549 potentiostat, while the cathode consisted of an activated titanium electrode (40 × 26 cm) provided by Industrie De Nora and placed close to the reactor inner wall. Cell voltage and current were monitored with two TTi 1604 digital multimeters. RR243 solution (25 mg L^{-1}) was continuously mixed by air bubbling at the bottom using an upward flow of 1.5 L h^{-1} cm^{-2}, and thermostated at 20 °C by an external cooling bath. Batch tests lasted 180 min and they were carried out 4 times, during which sample absorbance was moni-tored at RR243 characteristic wavelengths and at UV lamp emis-sion wavelength peak. RR243 mineralization was also evaluated by TOC analyses. The absence of relevant changes in chloride concentration during degradation test was verified.

2.5. Analytical methods

RR243 solution absorbance (254, 287, 515 and 545 nm), TOC, conductivity, pH and chloride concentration were measured according to Standard Methods (AWWA/APHA/WEF, 2012). Absorbance was measured by a Unicam UV–Vis 2 spectrophotometer (USA) with an optical path of 1 cm, while TOC was determined by a 3030 A Shimadzu TOC analyser. Conductivity and pH were monitored by Eutech pH 6+ (Thermo Scientific) and Eutech Cond 6+ (Thermo Scientific), respectively.

3. Results and discussion

3.1. Structural characterization of nanotubular TiO_2

An optical microscope image of the surface structure is reported in Fig. 3a, while an ESEM image of nanotubular TiO_2 is shown in Fig. 3b: film morphology is compact and uniform, its thickness is about 500–600 nm and the average diameter of nanotubes is approximately 100–150 nm. In the image, which refers to one of

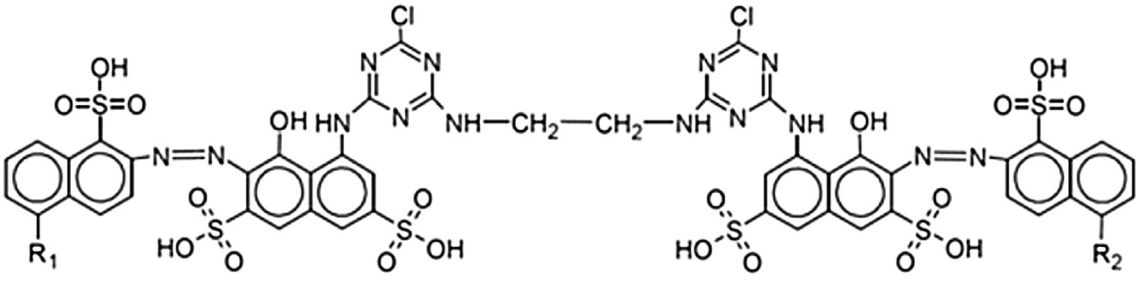

Fig. 1. Molecular structure of RR243. Three different molecular configurations are possible: (1) $R_1 = R_2 = SO_3H$ - (2) $R_1 = SO_3H$, $R_2 = H$ - (3) $R_1 = R_2 = H$.

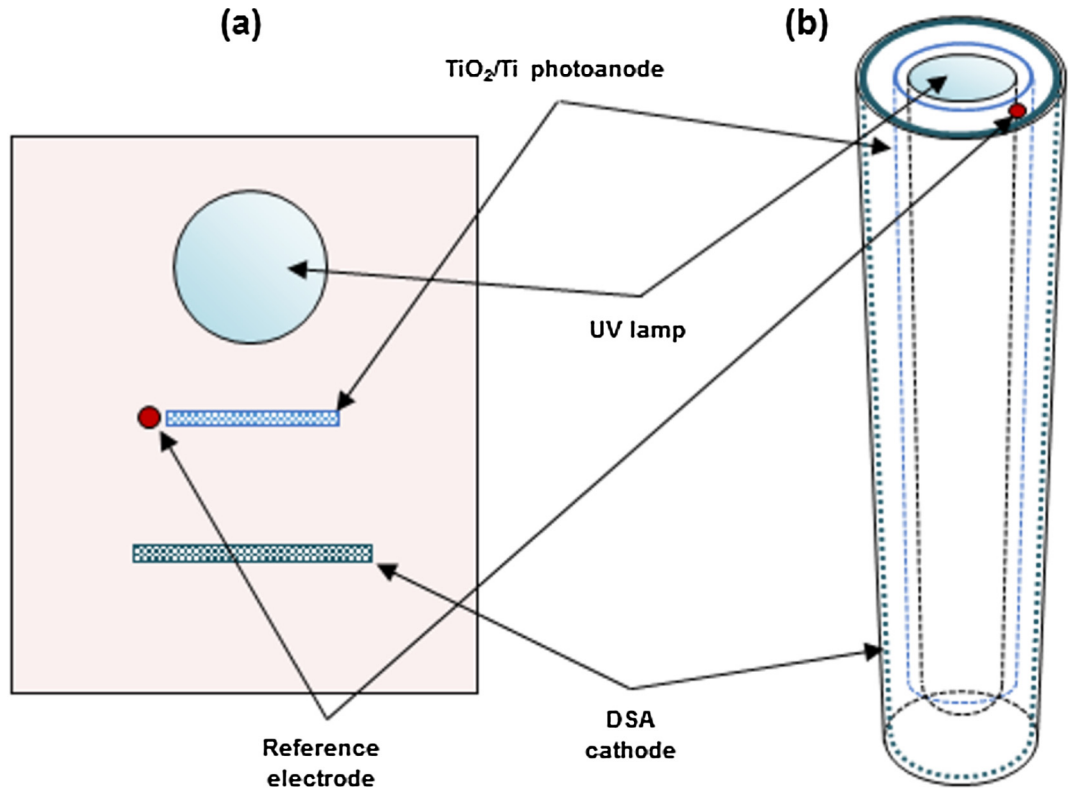

Fig. 2. Schematic representation of: (a) three-electrode cell for photoelectrochemical tests (top view); (b) optimized photoelectrocatalytic reactor for degradation tests (3D view).

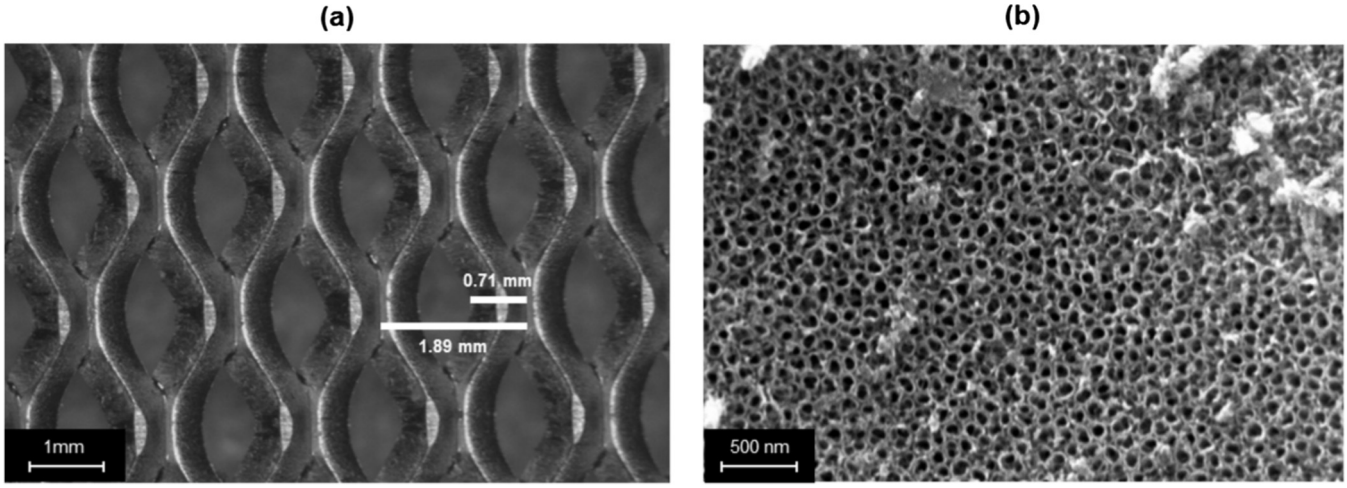

Fig. 3. (a) Titanium expanded metal (optical microscope) and (b) nanotubular TiO_2 (ESEM).

the cylindrical TiO_2/Ti samples, some deposits can be observed on TiO_2 surface. A geometric surface area of 1.3 cm^2 has been estimated per 1 cm^2 of apparent surface area for the expanded metal, according to the procedure in Supplementary Material (S1).

The XRD spectra of a sample before and after annealing is reported in Supplementary Material (S2). The change in TiO_2 crystalline structure can be clearly observed in terms of an increase of both anatase and rutile peaks after heat treatment. Using the method described by Jenkins and Snyder (2012), the percentage distribution of crystalline phases composing the oxide film was determined: anatase and rutile phases were respectively 70–80% and 20–30%.

3.2. Photoelectrochemical tests on nanotubular TiO_2

Photoelectrochemical tests were performed on nanotubular TiO_2 to measure the photocurrent, considered as a proxy variable. In fact, under stable operating conditions, an increase in photocurrent corresponds to an increase in the electron - hole separation on TiO_2 surface (Carp, 2004). Measurements were performed in potentiostatic and linear sweep potentiodynamic tests.

A stabilization phase was required under irradiation since the process reached the steady state after some minutes. In particular, characteristic trends in current have been observed as a function of polarization voltage: at 0 V the current displayed a peak and then

stabilized to a steady state value, while the initial peak decreases at increasing polarization voltage (0.5, 1.5 V). As an example, experimental data for current over time as a function of polarization voltage are shown in Supplementary Material (S3). For 1.5 V polarization voltage, the presence of a relevant current (about 350 μA) in dark condition can be noticed.

In the following, experimental results highlight the influence of the various operating parameters, namely polarization voltage, TiO_2 electrode relative positioning to UV source (distance) and RR243 concentration, on TiO_2 photoactivation.

3.2.1. Influence of polarization voltage

The effect of polarization voltage on nanotubular TiO_2 photoactivation was investigated both in potentiostatic and potentiodynamic conditions.

In potentiostatic tests, as shown in Tables 1 and 2, the polarization voltage enhanced photocurrent density of about 3–4 times for 0.5 V and 6–7 times for 1.5 V, irrespectively of TiO_2/Ti sample - UV lamp distance and RR243 concentration. In all cases photocurrent was proportional to the polarization voltage. The differences in photocurrent density varying TiO_2/Ti sample - UV lamp distance and RR243 concentration are due to changes in radiation delivered at TiO_2 surface, in turn related to radiative path and solution absorbance. In the view of enriching the discussion, some more elements related to the irradiation of nanotubular TiO_2 at the micro scale are given in Adán et al. (2016).

In potentiodynamic tests, the effect of polarization has been studied as a function of the polarization voltage, as reported in Fig. 4. Photocurrent density increased significantly for polarization voltage up to 0.3 V, while almost constant values were observed between 0.4 and 1.6 V.

Experimental results were comparable between potentiostatic and potentiodynamic tests at 0 V, while higher photocurrent density values were detected in potentiostatic tests, being the difference progressively more relevant with increasing the polarization voltage. In potentiodynamic tests the current could not reach steady state values because of the continuous variation in the polarization voltage. This hypothesis was verified by longer tests, in which the polarization voltage was increased more slowly (0.166 mV s^{-1}): a stronger enhancement in photocurrent density at increasing voltage was observed, but relevant RR243 degrada-tion was observed in trials lasting more than 45 min.

Accordingly, 1.5 V resulted as the optimum value for the photoactivation of nanotubular TiO_2. Higher potential values cause the electrolysis of water. Moreover, no damages of nanotubular TiO_2 were noticed in this condition, being this feature evaluated by means of ESEM images and in terms of performance stability during time. In detail, as for the latter aspect, the photoelectrochemical response of TiO_2/Ti samples was observed to be constant over long-duration testing (hundreds of hours). However, a case-by-case assessment is suggested since high values of current intensity can pose a risk for nanotubular TiO_2 integrity (Shankar et al., 2009).

3.2.2. Influence of nanotubular TiO_2 positioning with respect to the UV source

As reported in Table 1, the TiO_2/Ti sample - UV lamp distance determined a significant decrease in photocurrent density with increasing TiO_2/Ti sample distance from radiation source at fixed RR243 concentration. Moreover, as shown in Table 2, the higher was the RR243 concentration, meaning the lower was the transmittance at 254 nm, the steeper was the decrease of photocurrent density at fixed TiO_2/Ti sample - UV lamp distance, confirming that RR243 concentration negatively affects the radiation available for nanotubular TiO_2 photoactivation. Photocurrent density decreased accordingly to an exponential trend, in accordance with the Beer-Lambert law (Calvert and Pitts, 1966), which describes the transmission of radiation through a non-scattering liquid medium. Therefore, the following expression is proposed to describe the photocurrent density as a function of TiO_2/Ti sample - UV lamp distance and solution transmittance:

$$PC_x = PC_0 e^{-\delta x} \quad \text{(e.1)}$$

in which:

PC_x (μA cm^{-2}) = photocurrent density at x (cm) distance from UV lamp,
PC_0 (μA cm^{-2}) = photocurrent density at zero distance from UV lamp,
δ (cm^{-1}) = decay coefficient for photocurrent density.

The photocurrent density at a given distance from UV lamp is thus defined as a fraction of the photocurrent density generated by the TiO_2/Ti sample positioned at zero distance from UV lamp (PC_0). The decrease in the maximum photocurrent density is mathematically described by a dimensionless factor ranging between 0 and 1, which depends on the radiation optical path (x) and a photocurrent decay coefficient (δ), in turn a function of the solution optical properties.

3.2.3. Influence of RR243 concentration

Considering the proposed model (e.1), it can be assumed that the PC_0 value is the same irrespectively of RR243 concentrations: in fact, when the TiO_2/Ti sample is located closely to the UV lamp surface (x = 0 cm), the optical path is zero and therefore no attenuation phenomena occur. The model parameters (PC_0 and δ) were estimated at different polarization voltages and RR243 concentrations by non-linear regression and they are reported in Table 3 with the relative determination coefficients (R^2). At same RR243 concentration PC_0 values are similar: 37 ± 5.4, 121 ± 9.1 and 252± 22.7 μA cm^{-2} respectively for the three applied values of polarization voltage and the slight differences among PC_0 values are probably due to experimental errors. Otherwise, the values of δ coefficient increase exponentially as a function of RR243 concentration, according to the following equation:

$$\delta = \delta_0 e^{\gamma C} \quad \text{(e.2)}$$

Table 1
Photocurrent density (expressed as μA cm^{-2}) measured in potentiostatic tests as function of polarization voltage, TiO_2/Ti sample - UV lamp distance and RR243 concentration.

Polarization voltage (V)	RR243 concentration (mg L^{-1})	Distance (cm)						
		1	2	3	4	5	7	9
0	0	31.54	25.90	19.92	15.40	12.45	8.52	7.11
	25	9.25	2.28	0.36	0.12	0.06	0.00	0.00
0.5	0	108.24	87.89	67.96	50.59	38.90	27.97	20.69
	25	45.36	10.92	1.53	0.39	0.18	0.02	0.00
1.5	0	217.15	174.98	133.89	109.76	85.46	57.06	33.26
	25	75.19	15.05	2.32	0.82	0.27	0.00	0.00

Table 2
Photocurrent density (expressed as $\mu A\ cm^{-2}$) measured in potentiostatic tests as function of polarization voltage and RR243 concentration at fixed TiO_2/Ti sample – UV lamp distance (1 cm).

Polarization voltage (V)	RR243 concentration ($mg\ L^{-1}$)					
	0	5	10	15	20	25
0	31.54	24.36	20.13	15.87	12.17	9.25
0.5	108.24	82.56	70.54	59.93	46.42	45.36
1.5	217.15	170.63	150.36	121.53	101.66	75.19

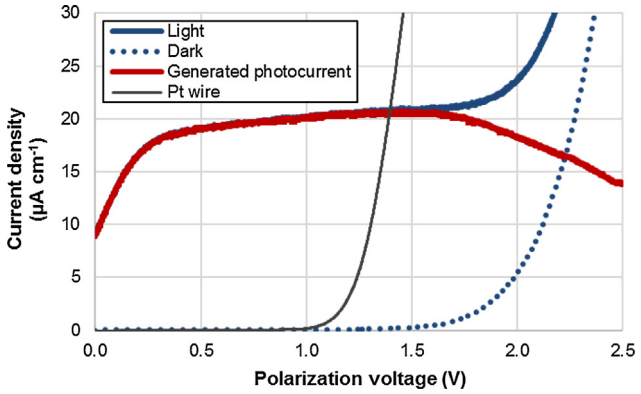

Fig. 4. Current density vs. polarization voltage in potentiodynamic tests for TiO_2/Ti sample (1 cm TiO_2 sample - UV lamp distance, 25 $mg\ L^{-1}$ RR243 concentration).

in which:

δ_0 (cm^{-1}) = decay coefficient for the photocurrent at zero RR243 concentration,
γ ($L\ mg^{-1}$) = factor for dependence of coefficient δ on RR243 concentration,
C ($mg\ L^{-1}$) = RR243 concentration.

The model parameters were estimated by the least square method for 0, 0.5 and 1.5 V, respectively getting the following equations: $\delta = 0.200e^{0.076C}$ ($R^2 = 0.996$), $\delta = 0.227e^{0.073C}$ ($R^2 = 0.990$), $\delta = 0.246e^{0.072C}$ ($R^2 = 0.995$). Then, by means of a sensitivity analysis, it was highlighted that polarization voltage marginally affects the δ_0 coefficient, while it has a negligible influence on γ, only depending on RR243 concentration and, thus, on the radiation delivered at TiO_2/Ti sample surface.

According to Eqs. (e.1) and (e.2), nanotubular TiO_2 photoactivation was simulated, in terms of PC_x/PC_0, as a function of TiO_2/Ti sample - UV lamp distance for various values of RR243 concentration at 1.5 V polarization voltage, being modelling outcomes reported in Supplementary Material (S4).

3.3. Reactor configuration optimization

Based on the experimental results obtained in photoelectrochemical tests about the effect of specific operating parameters, valuable indications can be drawn for photoreactor configuration and process optimization in case of nanotubular TiO_2:

- the polarization voltage has to be optimized representing a trade-off among conflicting goals (maximization of TiO_2 photoactivation, minimization of operating costs and TiO_2 protection),
- the distance between TiO_2/Ti photocatalyst and UV lamp has to be minimized,
- solution absorbance is essential in determining radiation transfer inside photoreactor volume.

When dealing with process optimization, basically two goals have to be pursued for maximizing the production of reactive species in a photoreactor for photocatalysis on immobilized TiO_2: increase the photocatalytic surface and enhance the extent of TiO_2 photoactivation by delivering the maximum amount of energy per surface unit area (Van Gerven et al., 2007). Since these two aspects can be quantitatively described by means of indepen-dent variables, the most efficient geometry for a photocatalytic reactor can be determined by a combined assessment of these two influencing factors. As for the estimation of the radiation transfer to TiO2 photocatalyst surface, several numerical or statis-tical methodologies were successfully applied (*inter alia:* Duran et al., 2010; Zazueta et al., 2013), but it is important to stress that the solution of the radiation transfer equation is a very complex

Table 3
PC_0 and δ coefficients, R^2 values for non-linear regression equations for photocurrent density at various operating conditions (polarization voltage, RR243 concentration).

Polarization voltage (V)	RR243 concentration ($mg\ L^{-1}$)	PC_0 ($\mu A\ cm^{-2}$)	δ (cm^{-1})	R^2
0	0	36.0	0.194	0.977
	5	32.4	0.314	0.991
	10	42.8	0.405	0.989
	15	40.2	0.635	0.999
	20	39.5	0.931	0.996
	25	28.5	1.314	0.978
0.5	0	127.0	0.212	0.984
	5	131.2	0.354	0.985
	10	107.5	0.445	0.974
	15	126.6	0.721	0.994
	20	114.1	0.989	0.986
	25	117.4	1.301	0.981
1.5	0	274.7	0.231	0.998
	5	260.6	0.364	0.996
	10	211.9	0.520	0.992
	15	245.2	0.773	0.989
	20	270.1	1.032	0.991
	25	250.6	1.417	0.985

task in case of photocatalyst complex morphology. Otherwise, photocurrent is a proxy variable depending on both photocatalytic surface and specific TiO_2 photoactivation, which can be easily measured and that can be valuably used as an indicator of the overall process efficiency.

In the present case, a simple and rigorous methodology for process optimization and photoreactor configuration was developed based on photocurrent. In particular, a single-lamp annular geometry based on cylindrical photocatalytic surface was studied. It is important to point out that such methodology can be extended to any form of immobilized TiO_2 provided on flat or meshed substrate. The meshed substrate was preferred here primarily because it allows the design of photoreactors in which the photocatalyst does not coincide with reactor walls and in which the various fluid compartments created by the photocatalytic surface are in contact.

The optimization consisted essentially in the determination of the radius of the cylindrical TiO_2/Ti surface resulting in the maximization of the photocurrent. In fact, the above-mentioned trade-off problem can be formulated as: an increase in the radius of the cylindrical TiO_2/Ti surface determines a linear increase in photocatalytic surface, against an exponential decrease in photocurrent density, in agreement with Eq. (e.1). Then, the measured photocurrent intensity, calculated as the product of photocatalytic surface and photocurrent density, was modelled as a function of TiO_2/Ti sample radius and RR243 concentration. As an example, modelling outcomes at 1.5 V polarization voltage as a function of RR243 concentration are shown in Fig. 5.

It can be noticed that the increase of photocatalytic surface prevails on the effect of TiO_2/Ti sample - UV lamp distance at zero RR243 concentration, unlike for higher RR243 concentration. As a consequence, the photocatalyst radius which maximizes photocurrent depends on RR243 in solution: the optimum is achieved at distance as close as possible to UV lamp surface, namely the quartz sleeve radius (1.7 cm).

3.4. Photoelectrocatalytic degradation tests

An optimized photoreactor configuration was developed and used for the degradation of a 25 mg L^{-1} RR243 solution. Cylindrical TiO_2/Ti surface was located at a distance of 0.55 cm from the UV lamp surface, chosen as the smallest distance allowing the lift of air bubbles in the annulus.

During degradation tests negligible changes in conductivity, pH and chloride concentration were observed. In any case, the release of chlorine gas would be very poor, if occurring, as this species is expected to be rapidly hydrolysed to HClO (Crittenden et al., 2012).

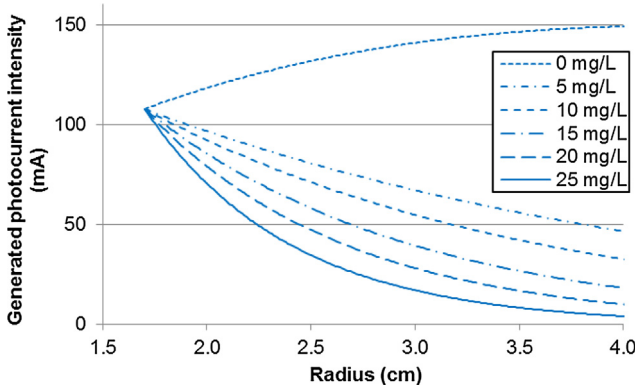

Fig. 5. Simulated photocurrent intensity vs. radius of the cylindrical TiO_2/Ti photocatalyst as a function of RR243 concentration at 1.5 V vs. Ag/AgCl.

Decolorization yields were expressed as the ratio of absorbances at a time t and time zero (ABS_t/ABS_0). Experimental results are reported in Fig. 6, where normalized absorbances at 515 and 545 nm are treated as a single set of data, as verified by means of a Student's *t*-test (p-value 0.05). 90% and 99% decolorization yields in the visible spectrum were reached respectively after about 45 and 60 min. Decolorization yields were significantly lower at 287 nm, leading to values of 90% for ABS_t/ABS_0 after about 90 min.

Experimental values of residual absorbance at 254 nm are shown in Fig. 6, highlighting both the effective degradation of RR243 and an improvement in solution transmittance during process time (passing from 33 ± 2.7% at the beginning of the experiments to 96 ± 4.0% after 120-min process time). This evidence is in agreement with the increase in photocurrent intensity monitored over time, shown in Fig. 6. In fact, photocurrent intensity increased from about 30 to 200 mA over 120 min. Therefore, a change in the operating conditions over process time was noticed, determining a continuous improvement of TiO_2 photoactivation and possibly resulting in accelerating kinetics for RR243 decolorization.

The difference in the decay of absorption values during process time at the four absorption wavelengths indicates that by-products are generated from the degradation of RR243 and that the decolorization proceeds with characteristic times different from those of by-products degradation, as also discussed in literature (Konstantinou and Albanis, 2004; Rauf and Ashraf, 2009).

Degradation yields were measured as the ratio between TOC concentration at a given time and initial TOC concentration (TOC_t/TOC_0). A linear decrease in TOC concentration was observed up to about 100 min (TOC_t/TOC_0 = 30–40%), while for longer process times the mineralization rate slowed down and stabilised at 70% mineralization after 120 min, probably due to the presence of highly refractory degradation by-products. The absence of relevant photolysis over process time was highlighted by specific tests (values lower than 5% at 515 and 545 nm after 120 min).

3.5. Decolorization kinetics

Langmuir-Hinshelwood kinetic has often been used for describing the photocatalytic degradation of pollutants, *inter alia* Toepfer et al. (2006) and Vezzoli et al. (2011), being this kinetic model accounting for pollutant adsorption on TiO_2 surface by a Langmuir mechanism according to the equation:

$$\frac{dC}{dt} = -k_R \cdot \frac{K_A C}{1 + K_A C} \qquad \text{(e.3)}$$

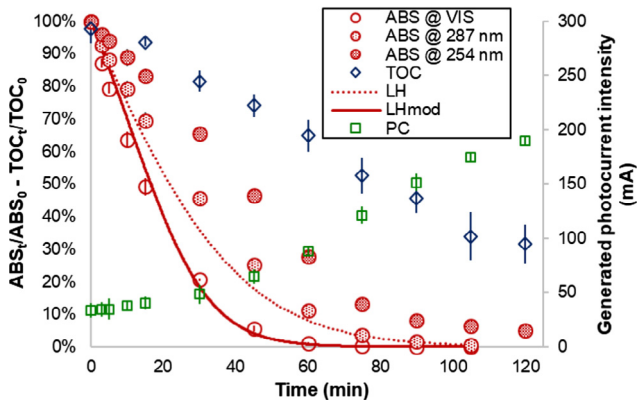

Fig. 6. Degradation of RR243 (25 mg L^{-1}) by photoelectrocatalysis on cylindrical TiO_2/Ti surface: residual solution absorbance (mean ± st.dev) at various wavelengths (VIS refers to 515 and 545 nm series) and residual TOC (mean ± st.dev) vs. time. Photocurrent intensity over process time is reported as well as data modelled by Langmuir-Hinshelwood (LH) and modified Langmuir-Hinshelwood (LHmod) kinetics.

in which:

k_R (mg L^{-1} min^{-1}) = Langmuir-Hinshelwood reaction constant,
K_A (L mg^{-1} min^{-1}) = equilibrium constant of adsorption.

First, in order to estimate kinetic model parameters, k_R and K_A, a model linearization, as described in a previous work (Turolla et al., 2015), was applied to experimental data referred to visible wavelengths. This procedure did not result in any successful outcome. Thus, kinetic model parameters were determined to obtain the best fitting of experimental data. As shown in Fig. 6, where the simulated residual values of RR243 concentration are plotted, the standard Langmuir-Hinshelwood model could not provide an effective description of experimental results. This is probably due to the already-introduced changing behaviour of the kinetics during process time, determined by the modification in solution transmittance and the consequent improvement in TiO_2 photoactivation.

Therefore, in order to effectively describe the mutable characteristics of the process, the standard Langmuir-Hinshelwood model was modified by introducing a dimensionless factor, f(C), in addition to the usual expression, as:

$$\frac{dC}{dt} = -f(C) \cdot k_R \cdot \frac{K_A C}{1 + K_A C} \quad \text{(e.4)}$$

Such factor was defined as a weighting factor for reaction constant k_R, since it provides information on the degradation rate of RR243 on TiO_2 surface, hence depending on TiO_2 photoactivation. In detail, f(C) assumes the minimum value, namely 1, at the beginning of the process, when RR243 concentration is maximum, and it increases during process time as a function of the change in RR243 concentration, until reaches the maximum value at the end of the process (minimum RR243 concentration). Therefore, the factor f(C) affects k_R positively over process time. As reported in Eq. (e.5), f(C) was defined as the ratio between photocurrent density corresponding to the RR243 concentration at a given time $PC(C_t)$ and the same variable at the beginning of the process $PC(C_0)$. Based on the formulation of photocurrent density proposed in Eqs. (e.1) and (e.2), $f(C_t)$ assumes the following expression:

$$f(C_t) = \frac{PC(C_t)}{PC(C_0)} = \frac{PC_0 e^{-\delta(C_t)x}}{PC_0 e^{-\delta(C_0)x}} = \frac{e^{-\delta(C_t)x}}{e^{-\delta(C_0)x}} = \frac{e^{-\delta_0 x e^{\gamma C_t}}}{e^{-\delta_0 x e^{\gamma C_0}}} = e^{\delta_0 x (e^{\gamma C_0} - e^{\gamma C_t})} \quad \text{(e.5)}$$

Particularly, $f(C_t)$ depends on decay coefficient for photocurrent at zero RR243 concentration (δ_0), radiation optical path (x), factor for dependence of coefficient δ on RR243 concentration (γ) and RR243 concentration over time. Being RR243 concentration the only changing variable (decreasing from 25 mg L^{-1}), the determination of $f(C_t)$ values resulted in values ranging from 1 to 1.9 over process time for the optimized photoreactor configuration (x = 0.55 cm) at 1.5 V. For the estimation, the previously-reported values of δ_0 and γ were adopted.

The proposed methodology is based on the assumption that the analytical method for the determination of the remaining RR243 concentration was not influenced by the generated by-products. In fact, if by-products absorb significantly at the same wavelengths as RR243, a reliable determination of RR243 concentration over process time is missing and the estimation of kinetic model parameters is affected by an error. As reported in Supplementary Material (S5), the absorption spectrum of the RR243 solution after 15-min process time and the absorption spectrum of a standard RR243 solution at the same remaining dye concentration, about 12.5 mg L^{-1}, were compared. No significant differences were observed between the absorption spectrum of the treated RR243 solution (including the absorption related to by-products) and the standard RR243 solution in the visible spectrum, indicating that no coloured by-products are generated in the process and, therefore, that no disturbance on the analytical method is expected.

As before, k_R and K_A were determined from experimental data in order to get the best fitting, obtaining 1.2 ± 0.25 mg L^{-1} min^{-1} and 0.05 ± 0.006 L mg^{-1}, respectively. The integration of the mod-ified Langmuir-Hinshelwood model, conducted by the Runge-Kutta method, led to a much better result in describing experimen-tal data than the standard formulation, as shown in Fig. 6, due to the effective description of the changing behaviour of the photocatalytic process over time.

The proposed kinetic model predicts a progressive increase of reaction rate up to an approximately doubling over process time, however the monitored photocurrent does not represent an effective indicator for degradation performance. In fact, photocurrent increased about 7 times and a relation with experimental results on RR243 was not observed. Hence, as already stated in the previous discussion about potentiodynamic tests, photocurrent can be adopted as proxy variable only under steady operating conditions.

Another remark concerns the neglecting of the influence of degradation by-products on the radiation transfer (Konstantinou and Albanis, 2004; Rauf and Ashraf, 2009). In fact, the modelling approach is based on assuming the scarce influence of these compounds on TiO_2 photoactivation.

In conclusion, the good prediction of experimental data constitutes a validation of the proposed modelling procedure based on photocurrent. The introduced methodology allows the modelling of the dynamic behaviour of the batch photocatalytic reactor and represents a generalizable framework, that could be easily adapted to other case-studies.

4. Conclusions

A simple and reliable methodology for process monitoring and optimization has been proposed and validated, allowing the definition of a single-lamp annular optimized configuration for a photoelectrocatalytic reactor using immobilized TiO_2 photocatalyst, namely nanotubular TiO_2 grown by anodic oxidation on Ti meshed substrate. Photocurrent was proved to be a useful indicator for the influence of operating parameters on TiO_2 photoactivation, characterized by ease of measurement, inexpensiveness and reliability. Photoelectrochemical response was modelled as a function of several operating parameters, namely polarization voltage, TiO_2/Ti surface positioning with respect to the UV source (distance) and RR243 concentration, and guidelines for photoreactor configuration were proposed. Anyway, photocurrent revealed to be effective only in steady state conditions. An optimized reactor configuration was developed and used for the degradation of an azo dye: 90% decolorization and 60% mineralization were achieved in 45 and 100 min, respectively. Langmuir-Hinshelwood kinetic model was mod-ified for describing the dynamic behaviour of the process over time due to modifications in optical properties of dye solution, which leads to an acceleration of decolourisation kinetics over time.

Acknowledgements

This work was partially funded by the Lombardia Region, Italy (grant ATP2009, project TITANO, ID 13726167). The valuable support of Massimo Fumagalli (Politecnico di Milano, Department of Chemistry, Materials and Chemical Engineering 'G. Natta') and Clelia Marchionna (Politecnico di Milano, Department of Mathematics) is greatly acknowledged.

Appendix A. Supplementary material

Supplementary data associated with this article can be found, in the online version, at https://doi.org/10.1016/j.ces.2018.02.041.

References

Adán, C., Marugán, J., Sánchez, E., Pablos, C., Van Grieken, R., 2016. Understanding the effect of morphology on the photocatalytic activity of TiO_2 nanotube array electrodes. Electrochim. Acta 191, 521–529.

Am. Water Work. Assoc., Am. Public Work. Assoc., Wat. Environ. Fed., 2012. Standard methods for the examination of water and wastewater.

Brugnera, M.F., Rajeshwar, K., Cardoso, J.C., Zanoni, M.V.B., 2010. Bisphenol A removal from wastewater using self-organized TiO_2 nanotubular array electrodes. Chemosphere 78, 569–575.

Calvert, J.G., Pitts, J.N., 1966. Photochemistry. John Wiley & Sons.

Cardoso, J.C., Lizier, T.M., Zanoni, M.V.B., 2010. Highly ordered TiO_2 nanotube arrays and photoelectrocatalytic oxidation of aromatic amine. Appl. Catal. B Environ. 99, 96–102.

Carp, O., 2004. Photoinduced reactivity of titanium dioxide. Prog. Solid State Chem. 32, 33–177.

Cheng, X., Liu, H., Yu, X., Chen, Q., Li, J., Wang, P., Umar, A., Wang, Q., 2013. Preparation of highly ordered TiO_2 nanotube array photoelectrode for the photoelectrocatalytic degradation of methyl blue: activity and mechanism study. Sci. Adv. Mater. 5, 1563–1570.

Choi, H., Al-Abed, S.R., Dionysiou, D.D., Stathatos, E., Lianos, P., 2010. TiO_2-based advanced oxidation nanotechnologies for water purification and reuse. Sustain. Sci. Eng. 2, 229–254.

Chong, M.N., Jin, B., Chow, C.W.K., Saint, C., 2010. Recent developments in photocatalytic water treatment technology: a review. Water Res. 44, 2997–3027.

Crittenden, J.C., Trussell, R.R., Hand, D.W., Howe, K.J., Tchobanoglous, G., 2012. Disinfection. In: MWH's Water Treatment. John Wiley & Sons.

De Lasa, H., Serrano, B., Salaices, M., 2005. Photocatalytic Reaction Engineering. Springer.

Duran, J.E., Mohseni, M., Taghipour, F., 2011. Computational fluid dynamics modeling of immobilized photocatalytic reactors for water treatment. AIChE J. 57, 1860–1872.

Duran, J.E., Taghipour, F., Mohseni, M., 2010. Irradiance modeling in annular photoreactors using the finite-volume method. J. Photochem. Photobiol. A Chem. 215, 81–89.

Egerton, T.A., Christensen, P.A., 2004. Photoelectrocatalysis processes. In: Parsons, S. (Ed.), Advanced Oxidation Processes for Water and Wastewater Treatment. IWA Publishing.

Fujishima, A., Zhang, X., Tryk, D., 2008. TiO_2 photocatalysis and related surface phenomena. Surf. Sci. Rep. 63, 515–582.

Garcia-Segura, S., Brillas, E., 2017. Applied photoelectrocatalysis on the degradation of organic pollutants in wastewaters. J. Photochem. Photobiol. C Photochem. Rev. 31, 1–35.

Jenkins, R., Snyder, R., 2012. Introduction to X-ray Powder Diffractometry. Wiley-InterScience.

Jennings, J.R., Ghicov, A., Peter, L.M., Schmuki, P., Walker, A.B., 2008. Dye-sensitized solar cells based on oriented TiO_2 nanotube arrays: transport, trapping, and transfer of electrons. J. Am. Chem. Soc. 130, 13364–13372.

José Martín de Vidales, M., Mais, L., Sáez, C., Cañizares, P., Walsh, F.C., Rodrigo, M.A., Rodrigues, C. de A., Ponce de León, C., 2016. Photoelectrocatalytic oxidation of methyl orange on a TiO_2 nanotubular anode using a flow cell. Chem. Eng. Technol. 39, 135–141.

Konstantinou, I.K., Albanis, T.A., 2004. TiO_2-assisted photocatalytic degradation of azo dyes in aqueous solution: kinetic and mechanistic investigations: a review. Appl. Catal. B Environ. 49, 1–14.

Leblebici, M.E., Stefanidis, G.D., Van Gerven, T., 2015. Comparison of photocatalytic space-time yields of 12 reactor designs for wastewater treatment. Chem. Eng. Process. Process Intensif. 97, 106–111.

Litter, M.I., 2009. Advances in Chemical Engineering - Photocatalytic Technologies. Elsevier.

Macak, J.M., Tsuchiya, H., Ghicov, A., Yasuda, K., Hahn, R., Bauer, S., Schmuki, P., 2007. TiO_2 nanotubes: self-organized electrochemical formation, properties and applications. Curr. Opin. Solid State Mater. Sci 11, 3–18.

Meng, Q., Wang, J., Xie, Q., Dong, H., Li, X., 2011. Water splitting on TiO_2 nanotube arrays. Catal. Today 165, 145–149.

Mor, G.K., Varghese, O.K., Paulose, M., Shankar, K., Grimes, C.A., 2006. A review on highly ordered, vertically oriented TiO_2 nanotube arrays: fabrication, material properties, and solar energy applications. Sol. Energy Mater. Sol. Cells 90, 2011–2075.

Pablos, C., van Grieken, R., Marugán, J., Adán, C., Osuna, M., Palma, J., 2013. Photoelectrocatalytic study and scaling up of titanium dioxide electrodes for wastewater treatment. Water Sci. Technol. 68, 999–1003.

Pichat, P., 2013. Photocatalysis and Water Purification: From Fundamentals to Recent Applications. Wiley-VCH.

Quan, X., Ruan, X., Zhao, H., Chen, S., Zhao, Y., 2007. Photoelectrocatalytic degradation of pentachlorophenol in aqueous solution using a TiO_2 nanotube film electrode. Environ. Pollut. 147, 409–414.

Rauf, M.A., Ashraf, S.S., 2009. Fundamental principles and application of heterogeneous photocatalytic degradation of dyes in solution. Chem. Eng. J. 151, 10–18.

Roy, P., Berger, S., Schmuki, P., 2011. TiO_2 nanotubes: synthesis and applications. Angew. Chemie Int. Ed. 50, 2904–2939.

Shankar, K., Basham, J.I., Allam, N.K., Varghese, O.K., Mor, G.K., Feng, X., Paulose, M., Seabold, J.A., Choi, K.-S., Grimes, C.A., 2009. Recent advances in the use of TiO_2 nanotube and nanowire arrays for oxidative photoelectrochemistry. J. Phys. Chem. C 113, 6327–6359.

Toepfer, B., Gora, A., Li Puma, G., 2006. Photocatalytic oxidation of multicomponent solutions of herbicides: reaction kinetics analysis with explicit photon absorption effects. Appl. Catal. B Environ. 68, 171–180.

Turolla, A., Fumagalli, M., Bestetti, M., Antonelli, M., 2012. Electrophotocatalytic decolorization of an azo dye on TiO_2 self-organized nanotubes in a laboratory scale reactor. Desalination 285, 377–382.

Turolla, A., Piazzoli, A., Budarz, J.F., Wiesner, M.R., Antonelli, M., 2015. Experimental measurement and modelling of reactive species generation in TiO_2 nanoparticle photocatalysis. Chem. Eng. J. 271, 260–268.

Van Gerven, T., Mul, G., Moulijn, J., Stankiewicz, A., 2007. A review of intensification of photocatalytic processes. Chem. Eng. Process. Process Intensif. 46, 781–789.

Varghese, O.K., Grimes, C.A., 2008. Appropriate strategies for determining the photoconversion efficiency of water photoelectrolysis cells: a review with examples using titania nanotube array photoanodes. Sol. Energy Mater. Sol. Cells 92, 374–384.

Vezzoli, M., Martens, W.N., Bell, J.M., 2011. Investigation of phenol degradation: true reaction kinetics on fixed film titanium dioxide photocatalyst. Appl. Catal. A Gen. 404, 155–163.

Wang, N., Li, X., Wang, Y., Quan, X., Chen, G., 2009. Evaluation of bias potential enhanced photocatalytic degradation of 4-chlorophenol with TiO_2 nanotube fabricated by anodic oxidation method. Chem. Eng. J. 146, 30–35.

Ye, Y., Feng, Y., Bruning, H., Yntema, D., Rijnaarts, H.H.M., 2018. Photocatalytic degradation of metoprolol by TiO_2 nanotube arrays and UV-LED: effects of catalyst properties, operational parameters, commonly present water constituents, and photo-induced reactive species. Appl. Catal. B Environ. 220, 171–181.

Zazueta, A.L.L., Destaillats, H., Li Puma, G., 2013. Radiation field modeling and optimization of a compact and modular multi-plate photocatalytic reactor (MPPR) for air/water purification by Monte Carlo method. Chem. Eng. J. 217, 475–485.

Zhang, Q., Zhu, J., Wang, Y., Feng, J., Yan, W., Xu, H., 2014. Electrochemical assisted photocatalytic degradation of salicylic acid with highly ordered TiO_2 nanotube electrodes. Appl. Surf. Sci. 308, 161–169.

Zhang, Y., Xiong, X., Han, Y., Zhang, X., Shen, F., Deng, S., Xiao, H., Yang, X., Yang, G., Peng, H., 2012. Photoelectrocatalytic degradation of recalcitrant organic pollutants using TiO_2 film electrodes: an overview. Chemosphere 88, 145–154.

Zhu, K., Neale, N.R., Miedaner, A., Frank, A.J., 2007. Enhanced charge-collection efficiencies and light scattering in dye-sensitized solar cells using oriented TiO_2 nanotubes arrays. Nano Lett. 7, 69–74.

Zlamal, M., Macak, J.M., Schmuki, P., Krýsa, J., 2007. Electrochemically assisted photocatalysis on self-organized TiO_2 nanotubes. Electrochem. Commun. 9, 2822–2826.